



Traditional medicinal plants against replication, maturation and transmission targets of SARS-CoV-2: computational investigation

Priya Mondal^{a,b*}, Jagadish Natesh^{a,b*}, Abdul Ajees^{a,b*}, Abdul Salam^c, Saravanamuthu Thiyagarajan^d and Syed Musthapa Meeran^{a,b}

^aDepartment of Biochemistry, CSIR-Central Food Technological Research Institute, Mysore, Karnataka, India; ^bAcademy of Scientific and Innovative Research (AcSIR), Ghaziabad, Uttar Pradesh, India; ^cDepartment of Atomic and Molecular Physics, Centre for Applied Nanosciences, Manipal Academy of Higher Education, Manipal, Karnataka, India; ^dInstitute of Bioinformatics and Applied Biotechnology (IBAB), Biotech Park, Electronic City Phase I, Electronic City, Bangalore, Karnataka, India

Communicated by Ramaswamy H. Sarma

ABSTRACT

COVID-19 is an infectious pandemic caused by the SARS-CoV-2 virus. The critical components of SARS-CoV-2 are the spike protein (S-protein) and the main protease (M^{Pro}). M^{Pro} is required for the maturation of the various polyproteins involved in replication and transcription. S-protein helps the SARS-CoV-2 to enter the host cells through the angiotensin-converting enzyme 2 (ACE2). Since ACE2 is required for the binding of SARS-CoV-2 on the host cells, ACE2 inhibitors and blockers have got wider attention, in addition to S-protein and M^{Pro} modulators as potential therapeutics for COVID-19. So far, no specific drugs have shown promising therapeutic potential against COVID-19. The current study was undertaken to evaluate the therapeutic potential of traditional medicinal plants against COVID-19. The bioactives from the medicinal plants, along with standard drugs, were screened for their binding against S-protein, M^{Pro} and ACE2 targets using molecular docking followed by molecular dynamics. Based on the higher binding affinity compared with standard drugs, bioactives were selected and further analyzed for their pharmacological properties such as drug-likeness, ADME/T-test, biological activities using *in silico* tools. The binding energies of several bioactives analyzed with target proteins were relatively comparable and even better than the standard drugs. Based on Lipinski factors and lower binding energies, seven bioactives were further analyzed for their pharmacological and biological characteristics. The selected bioactives were found to have lower toxicity with a higher GI absorption rate and potent anti-inflammatory and anti-viral activities against targets of COVID-19. Therefore, the bioactives from these medicinal plants can be further developed as phytopharmaceuticals for the effective treatment of COVID-19.

ARTICLE HISTORY

Received 21 July 2020
Accepted 21 October 2020

KEYWORDS

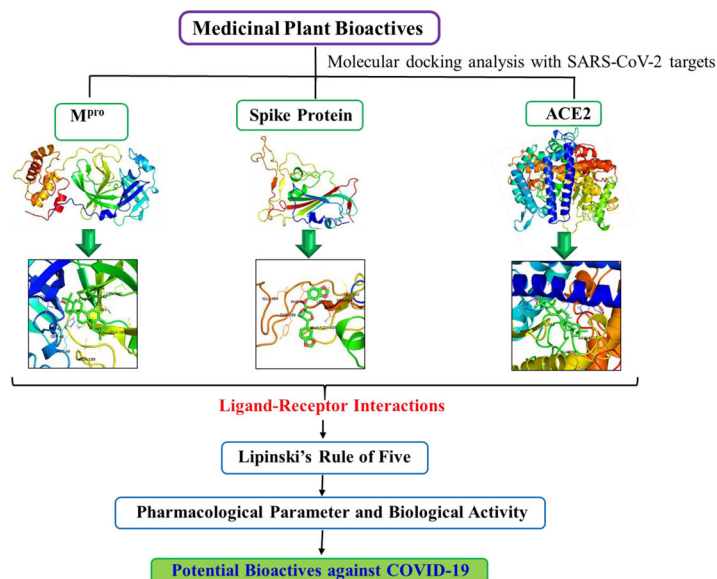
COVID-19; SARS-CoV-2;
molecular docking;
molecular dynamics;
medicinal plants

CONTACT Syed Musthapa Meeran ✉ s.musthapa@cftri.res.in 📧 Laboratory of Cancer Epigenetics, Department of Biochemistry, CSIR-Central Food Technological Research Institute (CSIR-CFTRI), Mysore, Karnataka 570020, India; Abdul Ajees Abdul Salam ✉ abdul.ajeesh@manipal.edu 📧 Department of Atomic and Molecular Physics, Centre for Applied Nanosciences, Manipal Academy of Higher Education, Manipal-576104, Karnataka, India.

*Equal contributors.

📄 Supplemental data for this article can be accessed online at <https://doi.org/10.1080/07391102.2020.1842246>.

© 2020 Informa UK Limited, trading as Taylor & Francis Group



Traditional medicinal plant bioactives can potentially inhibit SARS-CoV-2 protein targets. Computational investigation revealed that selected medicinal plant bioactives have the optimal pharmacological and biological activities against COVID-19.

1. Introduction

Coronavirus disease (COVID-19) is an infectious disease caused by the Severe Acute Respiratory Syndrome Coronavirus 2 (SARS-CoV-2) from the Coronaviridae family and declared as a global pandemic by World Health Organization on 11 March 2020. The new strain of SARS-CoV-2 has lesser virulence but more contagious than its predecessors SARS-CoV and MERS-CoV (Vellingiri et al., 2020). The highly infectious nature of the COVID-19 is due to the molecular evolution that occurred in the genome of SARS-CoV-2 (Andersen et al., 2020). SARS-CoV-2 is a *Betacoronavirus* belonging to the family of enveloped positive single-stranded RNA. SARS-CoV-2 comprises four major structural proteins; among them, spike glycoprotein (S-protein) is an essential protein, involved in the receptor-host selectivity and infection to the host. The S-protein contains the S1 and S2 subunits, S1 subunit functions as the receptor-binding domain, and involved in binding with the host receptor. Whereas the S2 subunit is engaged in the fusion of viral membrane with the host cellular membrane (Lan et al., 2020; Shang et al., 2020). S-protein selectively recognizes human angiotensin-converting enzyme 2 (ACE2) receptor and transmits the virus into the host cell. Intriguingly, the S-protein of SARS-CoV-2 has shown a higher affinity towards the ACE2 receptor compared with SARS-CoV (Lan et al., 2020; Shang et al., 2020). The stronger association of S-protein with ACE2 might be one of the reasons behind the higher infectious efficiency of SARS-CoV-2. Apart from structural proteins, the Main protease (M^{Pro}) is a non-structural protein and acts as a critical component of the SARS-CoV-2 viral life

cycle. M^{Pro} is a cysteine protease involved in the proteolytic maturation of various polypeptides into non-structural proteins, which are involved in replication and transcription (Jin et al., 2020). Thus, the functionalities of M^{Pro}, S-protein and ACE2 receptor grasp attention as potential therapeutic targets against COVID-19.

The primary symptoms of COVID-19 include fever, dry cough, fatigue, headache and diarrhea (Lan et al., 2020). As the SARS-CoV-2 infection progresses, a hyperinflammatory reaction is mediated through exaggerated cytokine response, intense lymphopenia, as well as considerable mononuclear cell infiltration into the various organs (Merad & Martin, 2020). The mortality owing to COVID-19 is mainly due to the clinical features in the advanced stages like acute respiratory distress syndrome and severe cardiac injury (Bonow et al., 2020). Currently, there is a lack of specific anti-viral therapeutics and vaccines against COVID-19 (Rodríguez-Morales et al., 2020). Some clinical studies have aimed to explore the available protease inhibitors, anti-HIV, anti-inflammatory and anti-malarial drugs. However, there is no evidence of the prophylactic and therapeutic effect of these drugs to overcome the morbidity and mortality caused by COVID-19.

Human civilization has been marred with the occurrence of epidemic and pandemics like SARS-CoV. At the same time, the 'survival of the fittest' taught to develop treatment practices and medicines within the natural bounty. 'Ayurveda' is one of the traditional Indian medicinal practices that has appealed attention as complementary approaches against various diseases, including viral infection (Mukhtar et al., 2008). Medicinal plant extracts are known to act as antipyretics, anti-inflammatory, expectorant, analgesic, etc. Several

Table 1. Binding energies (BEs; kcal/mol) of selected bioactives from medicinal plants with SARS-CoV-2 M^{Pro}, S- protein and human ACE2 and their chemical interactions with the binding site.

Medicinal plants and its bioactives	SARS-CoV-2 M ^{Pro}			SARS-CoV-2 S-protein			Human ACE2		
	BE	H-bond	Non-bonded Interactions	BE	H-bond	Non-bonded interactions	BE	H-bond	Non-bonded interactions
Amla (<i>Embllica officinalis</i>) Pedunculagin	-8.9	Thr26, His41, Ser46, Cys145, His163	Thr25, Met49, Phe140, Leu141, Asn142, Gly143, Met165, Glu166, Gln189	-7.7	Gln493, Ser494, Gly496, Asn501	Arg403, Glu406, Lys417, Tyr453, Leu455, Tyr505	-7.2	Asp30, His34, Asp38, Ala386	Asn33, Glu37, Ala387, Arg393
Amla (<i>Embllica officinalis</i>) Puniguconin	-8.5	Thr24, Thr25, Cys44, Phe140, His163, Glu166	Thr26, His41, Thr45, Ser46, Met49, Asn142, Gly143, Cys145, His164, Met165, His172, Gln189	-7.9	Arg403, Glu406, Gln409, Lys417, Tyr453, Gln493, Gln496	Tyr449, Leu455, Ser494, Tyr495, Tyr505	-6.6	Glu37, Asp38, Ala386, Ala387, Arg393	Asn33, His34, Lys353, Gln388, Pro389
Arni (<i>Clerodendrum indicum</i>) Taraxerol	-7.2	-	Thr24, Thr25, Thr26, Met49, Leu141, Asn142, Gly143, His164, Met165, Glu166, Gln189	-7.9	-	Leu452, Leu455, Glu484, Tyr489, Phe490, Leu492, Gln493	-7.0	Glu35, Gln76	Ser19, Gln24, Thr27, Phe28, Lys31, Leu79, Tyr83
Dhatura (<i>Datura innoxia</i>) Daturaolone	-7.3	-	Thr25, Thr26, Leu27, His41, Met49, Asn142, Gly143, Cys145, Glu166, Gln189	-7.5	-	Leu452, Leu455, Phe456, Tyr489, Phe490, Leu492, Gln493, Ser494	-7.0	His34	Asp38, Tyr41, Gln42, Leu45, Lys353
Dhatura (<i>Datura innoxia</i>) Withametelin	-7.9	-	Thr26, His41, Met49, Asn142, Gly143, Met165, Glu166, Gln189	-8.0	-	Leu452, Phe456, Glu484, Tyr489, Phe490, Leu492, Gln493, Ser494	-7.3	-	Asn33, His34, Glu37, Asp38, Lys353, Pro389, Arg393
Gaduchi (<i>Tinospora cordifolia</i>) Tinosporide	-8.5	Asn142, Glu166	His41, Met49, Tyr54, Leu141, Gly143, Ser144, Cys145, His164, Met165, His172, Asp187, Gln189	-6.4	Arg403, Arg408	Asp405, Glu406, Gln409, Gly416, Lys417, Tyr453	-6.5	His34	Asp38, Tyr41, Lys353
Haritaki (<i>Terminalia chebula</i>) Chebulagic acid	-6.5	Thr24, Thr26, Ser46, Asn142, Gly143, Gln189	Thr25, His41, Met49	-7.5	Arg403, Glu406, Tyr453, Gln493, Gly496	Lys417, Tyr449, Ser494, Tyr495, Tyr505	-6.6	Lys353	His34, Glu35, Glu37, Asp38, Tyr41, Arg393
Haritaki (<i>Terminalia chebula</i>) Chebulinic acid	-8.6	Thr24, Thr25, Cys44, Leu141, Asn142, Ser144, His163,	Thr26, Leu27, Thr45, Met49, Phe140, Gly143, Met165,	-6.5	Arg403, Tyr453, Phe490, Gln493, Gly496	Lys417, Tyr449, Leu455, Phe456, Tyr489, Ser494, Tyr505	-6.8	Glu35, Glu37, Asp38, Arg393	His34, Tyr41, Lys353

(continued)

Table 1. Continued.

Medicinal plants and its bioactives	SARS-CoV-2 M ^{pro}			SARS-CoV-2 S-protein			Human ACE2		
	BE	H-bond	Non-bonded Interactions	BE	H-bond	Non-bonded interactions	BE	H-bond	Non-bonded interactions
Haritaki (<i>Terminalia chebula</i>) Gallotannins	-8.3	Thr24, Phe140, Gly143, His164, Arg188	His172, Gln189 Thr25, Thr26, His41, Met49, Leu141, Asn142 Cys145, Met165, Glu166, Gln189	-7.4	Arg403, Glu406, Tyr453, Leu492, Gln493, Gly496	Lys417, Leu455, Phe456, Tyr489, Phe490, Ser494, Tyr495	-7.1	His34, Asp38, Ala387, Arg393	Asn33, Glu37, Tyr41, Lys353, Ala386, Gln388, Pro389
Indian Catmint (<i>Anisomeles indica</i>) Echinacin	-8.9	Thr24, Phe140, His164, Glu166, Arg188, Thr190, Gln192	Thr25, Thr26, His41, Met49, Asn142, Cys145, Met165, Gln189	-7.9	Glu484, Phe490	Tyr449, Leu452, Leu455, Phe456, Tyr489, Ser494	-7.8	Glu37, Gln96, Ala386, Ala387, Gln388, Arg393	Leu29, Asp30, Asn33, His34, Asp38, Tyr41, Val93, Lys353, Pro389
Indian ginseng (<i>Withania somnifera</i>) Withanolide A	-8.2	Thr26, His41, Glu166	Thr25, Met49, Phe140, Leu141, Asn142, Gly143, His164, Met165, Gln189	-7.7	Glu484	Leu452, Phe456, Tyr489, Phe490, Leu492, Gln493, Ser494	-7.0	Phe390, Arg393	Asn33, His34, Glu37, Asp38, Lys353, Pro389
Liquorice (<i>Glycyrrhiza glabra</i>) Glycyrrhizin	-8.2	Thr24, Thr25, Thr26, His41, Thr45, Ser46, Gln189	Leu27, Met49, Tyr118, Leu141, Asn142, Gly143, Cys145	-7.1	Arg403, Gln409, Lys417, Tyr449, Gln493, Gly496, Asn501	Tyr453, Tyr495, Tyr505	-7.0	His34, Asp38, Lys68	Glu35, Glu37, Leu39, Ala71, Phe72, Glu75, Lys353
Porcupine flower/Vajradanti (<i>Barleria prionitis</i>) Barlerinoside	-7.5	Thr24, Thr26, Leu141, Gly143, Ser144, Glu166, Gln189	Thr25, Leu27, Ser46, Met49, Phe140, Asn142, Cys145, His163, Met165, Thr190	-7.4	Arg403, Glu406, Gln409, Phe490, Gln493, Gly496, Asn501	Asp405, Lys417, Try449, Tyr453, Leu455, Phe456, Tyr489, Ser494, Tyr505	-6.5	Asp30, Lys31, Glu35, Asp38, Ala387	Asn33, His34, Glu37, Leu39, Tyr41, Lys353, Gln388, Pro389, Arg393
Sage-leaved alangium (<i>Alangium salvifolium</i>) Deoxytubulosine	-8.1	Cys145	Thr24, Thr25, Thr26, His41, Met49, Phe140, Leu141, Gly143, Met165, Glu166, Asp187, Gln189	-7.2	Leu492	Leu455, Phe456, Glu484, Gly485, Tyr489, Phe490, Gln493, Ser494	-6.9	-	Asn33, His34, Glu37, Asp38, Lys353, Gln388, Pro389, Arg393
White teak (<i>Gmelina arborea</i>) Quercetin 3-O-robinobioside	-8.8	Thr26, Asn142, Gly143, His163, Glu166, Thr190	Thr25, Leu27, Phe140, Cys145, His164, Met165, Arg188, Gln189	-7.9	Arg403, Glu406, Ser494, Gly496, Tyr505	Lys417, Tyr453, Leu455, Phe456, Tyr495, Phe497	-6.2	Phe28, Lys31, Glu35, Glu75, Gln76	Thr27, Leu79, Met82, Tyr83

Bioactives are written in boldface.

studies have also shown bioactives from medicinal plants function as potential anti-viral agents by boosting the inherent immune system (Ganjhu et al., 2015; Mukhtar et al., 2008). Furthermore, the anti-inflammatory properties of medicinal plants can reduce severe respiratory distress syndrome and acute cardiac injury, which are the leading cause

of COVID-19 morbidities (Cornélio Favarin et al., 2013; Liperoti et al., 2017). It is known that more than 25,000 plant-based formulations have been used in traditional Indian medicine (Vellingiri et al., 2020). Traditional medicines often pioneered the discovery of modern drugs yet underestimated due to the latter's target specificity and translational

Table 2. Predicted inhibition constant (Ki) of the selected medicinal plant bioactives and standard drugs against SARS-CoV-2 M^{Pro}, S-protein and human ACE2.

Bioactives	Inhibition constant (Ki) in μM		
	SARS-CoV-2 M ^{Pro}	SARS-CoV-2 S-protein	Human ACE2
Pedunculagin	0.31	2.31	5.36
Punigluconin	0.60	1.65	14.74
Taraxerol	5.36	1.65	7.51
Daturaolone	4.53	3.23	7.51
Withametelin	1.65	1.39	4.53
Tinosporide	0.60	20.64	14.74
Chebulagic acid	17.44	3.23	14.74
Chebulinic acid	0.51	17.44	10.52
Gallotannins	0.84	3.83	6.34
Echinacin	0.31	1.65	1.95
Withanolide A	0.99	2.31	7.51
Glycyrrhizin	0.99	6.34	7.51
Barlerinoside	3.23	3.83	17.44
Deoxytubulosine	1.18	5.36	8.89
Quercetin 3-O-robinobioside	0.36	1.65	28.92
Darunavir*	3.83	94.11	40.51
Dexamethasone*	10.52	20.64	12.45
Favipiravir*	306.26	218.61	507.82
Nelfinavir*	0.84	14.74	20.64
Remdesivir*	5.36	14.74	20.64
Enalapril*	–	–	79.51
Losartan*	–	–	28.92
Olmesartan*	–	–	34.23

*The standard drugs are marked as.

potential. Unlike modern medicine, a single herb may contain many bioactives that may function alone or in combinations to produce the desired relief. Therefore, in the present study, we investigated the therapeutic prospects of bioactives from the traditional medicinal plants against COVID-19.

2. Materials and methods

2.1. Preparation of ligands and receptors

Approved drugs for the treatment of HIV (Darunavir, Favipiravir, Nelfinavir, Remdesivir), ACE2 inhibitors (Enalapril, Losartan, Olmesartan) and Dexamethasone were chosen as the standard drugs for docking against SARS-CoV-2 M^{Pro}, S-protein and ACE2 receptor proteins (Supporting Information Table S1). The standard drugs were selected based on the existing anti-viral activities and ongoing clinical trials against SARS-CoV-2. Based on the literature evidences, 60 bioactives from 22 medicinal plants were selected for docking studies with SARS-CoV-2 M^{Pro}, S-protein and ACE2 receptor proteins (Supporting Information Table S2). The structural information of ligands, including eight standard drugs and sixty bioactives from the medicinal plants, were retrieved from PubChem (<https://pubchem.ncbi.nlm.nih.gov/>) database (Kim et al., 2019). The ligands were converted from 2D to 3D using Marvin sketch and Open Babel software tools (O'Boyle et al., 2011) (MarvinSketch, (<https://www.chemaxon.com>)). Further, ligand molecules were processed and converted into PDBQT file format using AutoDock Tools (v.1.5.6) of the MGL software package.

Receptor PDB structures of the SARS-CoV-2 M^{Pro} (PDB ID: 6LU7, Resolution: 2.16 Å; Jin et al., 2020), SARS-CoV-2 S-protein (PDB ID: 6W41, Resolution: 3.08 Å; Yuan et al., 2020) and

Human ACE2 (PDB ID: 1R42, Resolution: 2.20 Å; Towler et al., 2004) protein molecules were retrieved from protein data bank (PDB: www.rcsb.org). Protein molecules were prepared by removing water molecules and cofactors, adding polar H bonds and charges using ADT (Morris et al., 2009).

2.2. Molecular docking

Molecular docking of standard drugs and bioactives from medicinal plants with receptor molecules was performed using AutoDock Vina (Trott & Olson, 2010). The catalytic site of SARS-CoV-2 M^{Pro} (His41 and Cys145), receptor binding motif of S-protein (Leu455, Phe486, Glu493 and Ser494) and hotspot binding residues of ACE2 receptor (Lys31 and Lys353) were chosen as binding sites for docking analysis (Jin et al., 2020; Lan et al., 2020; Shang et al., 2020; Veeramachaneni et al., 2020; Yan et al., 2020). Grid box was generated using ADT with dimensions relative to the ligands (XYZ) with a resolution of 1 Å. The prepared ligand and receptor files were submitted to AutoDock Vina (Trott & Olson, 2010). Each docking calculations were repeated three times using different seeds and retaining the remaining values as default. Final protein-ligand interactive models were chosen based on the binding affinity as well as the molecular contacts. The hydrogen bond (H-bond), hydrophobic contacts were calculated using LigPlot+ (Laskowski & Swindells, 2011). The binding energy (BE) for each ligand-receptor docked complexes was obtained, and 2D conformations were generated using LigPlot+. Further, the inhibition constant (Ki) for standard drugs and medicinal plant bioactives with SARS-CoV-2 protein targets was determined using the following equation (Onawole et al., 2018).

$$K_i = 10^{(\text{Binding energy}/1.366)}$$

2.3. Screening of ligands based on drug-likeness properties

The drug-likeness properties of the standard drugs and selected medicinal plant bioactives were screened using Lipinski's rule of five (RO5; <http://www.scfbio-iitd.res.in/software/drugdesign/lipinski.jsp>; Lipinski, 2004). Additional drug-likeness features, including lipophilicity, solubility and the drug-likeness score of the ligands were obtained using OSIRIS Property Explorer (<https://www.organic-chemistry.org/prog/peo/>) and the SWISSADME server (<http://www.swissadme.ch/>; Daina et al., 2017).

2.4. ADME/Toxicity prediction of the selected ligands

The ADME/T predictions of bioactive ligands from the medicinal plants and standard drugs were analyzed by the application of the ADMETlab server (<http://admet.scbdd.com>). The achieved categorical and numerical values were converted into qualitative units based on explanations and interpretations provided by the ADMETlab server (Dong et al., 2018).

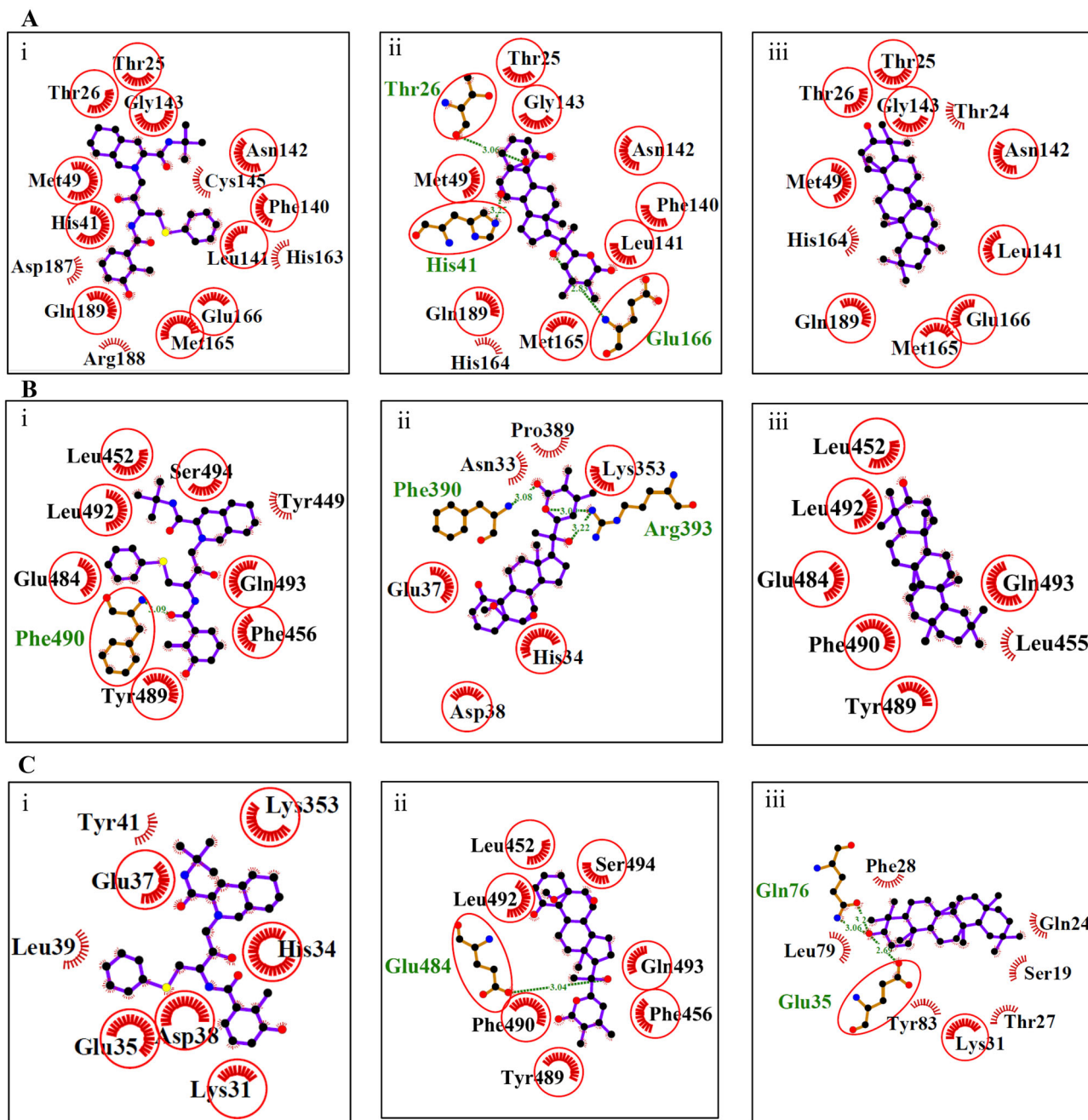


Figure 1. The 2D interaction plots displaying the interacting and common amino acids of the target proteins with the standard drug nelfinavir (i), and medicinal plant bioactives withanolide A (ii), taraxerol (iii). (A) MPTO catalytic dyad, (B) S-protein receptor-binding motif, (C) ACE2 receptor. The amino acids of target proteins within 4 Å proximity are shown, and the hydrogen bonds are represented in dotted lines and colored in green. Hydrophobic contacts are illustrated by an arc with spokes radiating towards the ligand atoms. Common amino acids are shown within red circles.

2.5. Prediction of adverse and toxic effects of ligands

The toxic properties including LD₅₀ of the ligands from medicinal plants were analyzed using the ProTox-II server (http://tox.charite.de/prottox_ii/) and OSIRIS Property Explorer (<https://www.organic-chemistry.org/prog/peo>). To predict the toxicity class and LD₅₀, the Canonical SMILES of ligands were submitted to the ProTox-II server (Drwal et al., 2014). The LD₅₀ values of standard drugs were retrieved from the DrugBank (<http://go.drugbank.com>) and Cayman chemical websites (<https://www.caymanchem.com/>). Other toxicity parameters of both standard drugs and bioactives from medicinal plants were predicted through OSIRIS Property Explorer.

2.6. Prediction of biological activity of ligands

The biological activity scales for the ligands of medicinal plants and standard drugs were predicted by using the Prediction of Activity Spectra for Substances (PASS) program (Filimonov et al., 2014). Briefly, the Canonical SMILES of ligands were used in the PASS-Way2Drug server (<http://www.pharmaexpert.ru/passonline/>) to predict the probability to be active (Pa) and the probability of becoming inactive (Pi). The bioactivity score (BAS) for the selected bioactives from medicinal plants and standard drugs was predicted using Molinspiration web-based tool (<http://www.molinspiration.com/cgi-bin/properties>). This web-based tool provides BAS

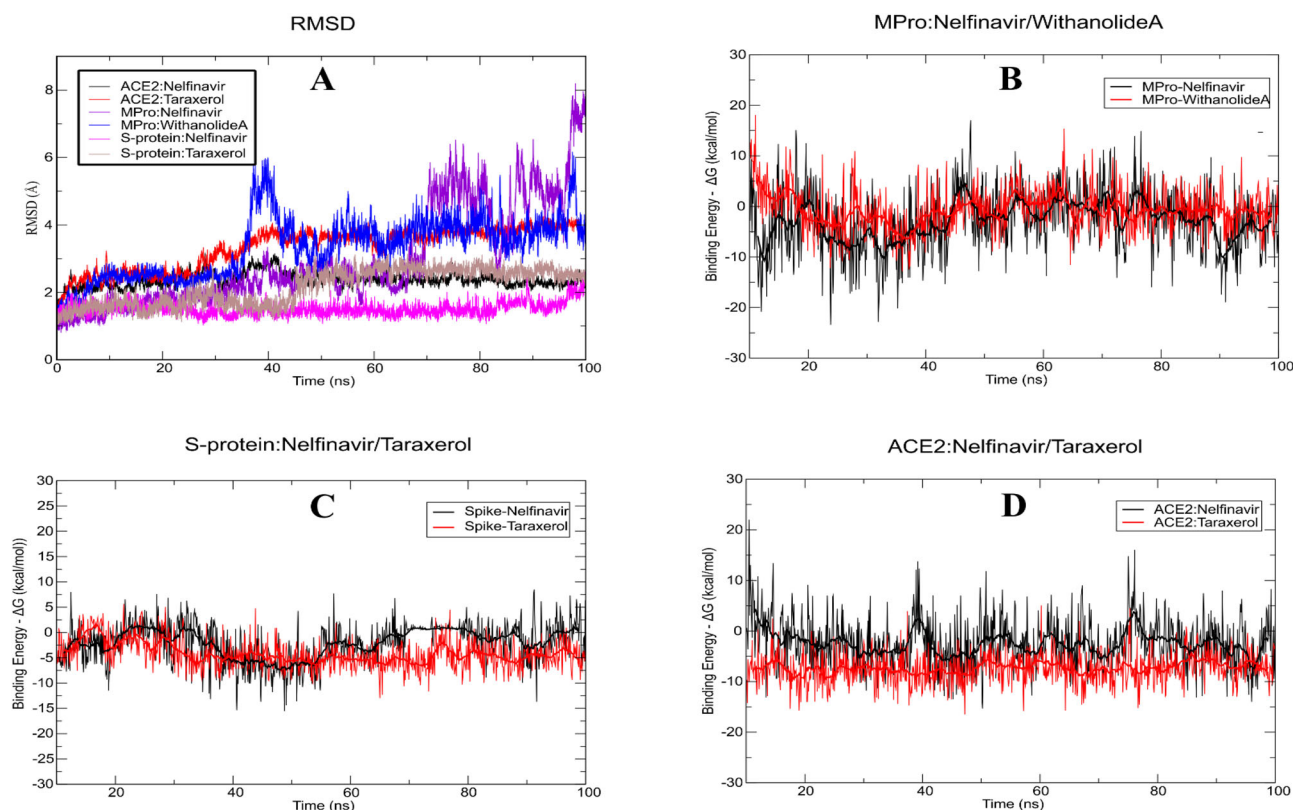


Figure 2. MD simulation and MM-PBSA analysis: (A) Root mean square deviation in the positions of protein backbone atoms (in angstrom units) during the MD simulation as superposed with their respective starting structures, calculated over 100 ns trajectory. Series color codes are given in the embedded box. Binding energy (kcal/mol) calculated by MM-PBSA analysis calculated from 10 to 100 ns of the MD simulations of (B) M^{Pro}:nelfinavir (black) and M^{Pro}:withanolide A (red) complex structures, (C) S-protein:nelfinavir (black) and S-protein: taraxerol (red) complex structure and (D) ACE2-nelfinavir (black) and ACE2-taraxerol (red) complex structures.

against human receptors and protein molecules like GPCRs, ion channels, nuclear receptors, proteases and kinases.

2.7. Molecular dynamics simulations

The molecular dynamics (MD) simulations were performed on three proteins, M^{Pro}, S-protein and ACE2 receptor proteins. Nelfinavir was selected as a common inhibitor, as it has shown a higher binding affinity with all the three target proteins. In addition to that based on the binding energies of selected bioactives from medicinal plants, withanolide A was taken for M^{Pro}, and taraxerol was taken for both S-protein and ACE2 to perform MD. The MD simulations were performed using the AMBER20 package (Case et al., 2020). The ff14SB forcefields were applied for proteins and ions, respectively. The antechamber program was used to develop force-field for all inhibitors using the gaff2 force field. The topology and coordinated files for protein and complex were created using the *tleap* program. For each complex system including protein and the ligand, TIP3P water molecules were placed in a 12 Å cubic box in each direction from the surface of the protein. To neutralize the system, 4 Na⁺, 2 Cl⁻ and 28 Na⁺ ions were added to M^{Pro}, S-protein and ACE2 proteins, respectively. The combined system was submitted to *sander* for energy minimization in four stages, using 5000 cycles steepest descent algorithm. For heating, the NVT ensemble was employed, and the temperature was gradually

increased until it reached 300 K. Langevin dynamics (thermostat) with a collision frequency of 2.0 ps⁻¹ were employed. For the equilibration phase, the NPT ensemble was employed. The SHAKE algorithm was employed to restrict the protein backbone atoms, while inhibitor and solvent molecules allowed free movement. Further, the well-equilibrated complex molecules M^{Pro} with nelfinavir, M^{Pro} with withanolide A, S-protein with nelfinavir, S-protein with taraxerol, ACE2 with nelfinavir and ACE2 with taraxerol were subjected to the production phase without any restraints for 100 ns MD with a time step of 2 fs. Coordinates and energy parameters were saved every 2 ps during the simulation for downstream analysis. The root means square deviation (RMSD) and hydrogen bond analysis were calculated using the *CPPTraj* module on the trajectories obtained.

2.8. Binding free energy calculations

The binding free energy of the protein-inhibitor complexation (ΔG) was calculated using molecular mechanics generalized Born surface area (MM-GBSA) and molecular mechanics Poisson-Boltzmann surface area (MM-PBSA). These classical methods were used to evaluate the energy difference between the two ends states of the system such as bound and unbound. These methods are also allowed to perform a more accurate analysis of residue wise contribution to the overall binding of the ligand to a receptor. The BE comprises of bonds,

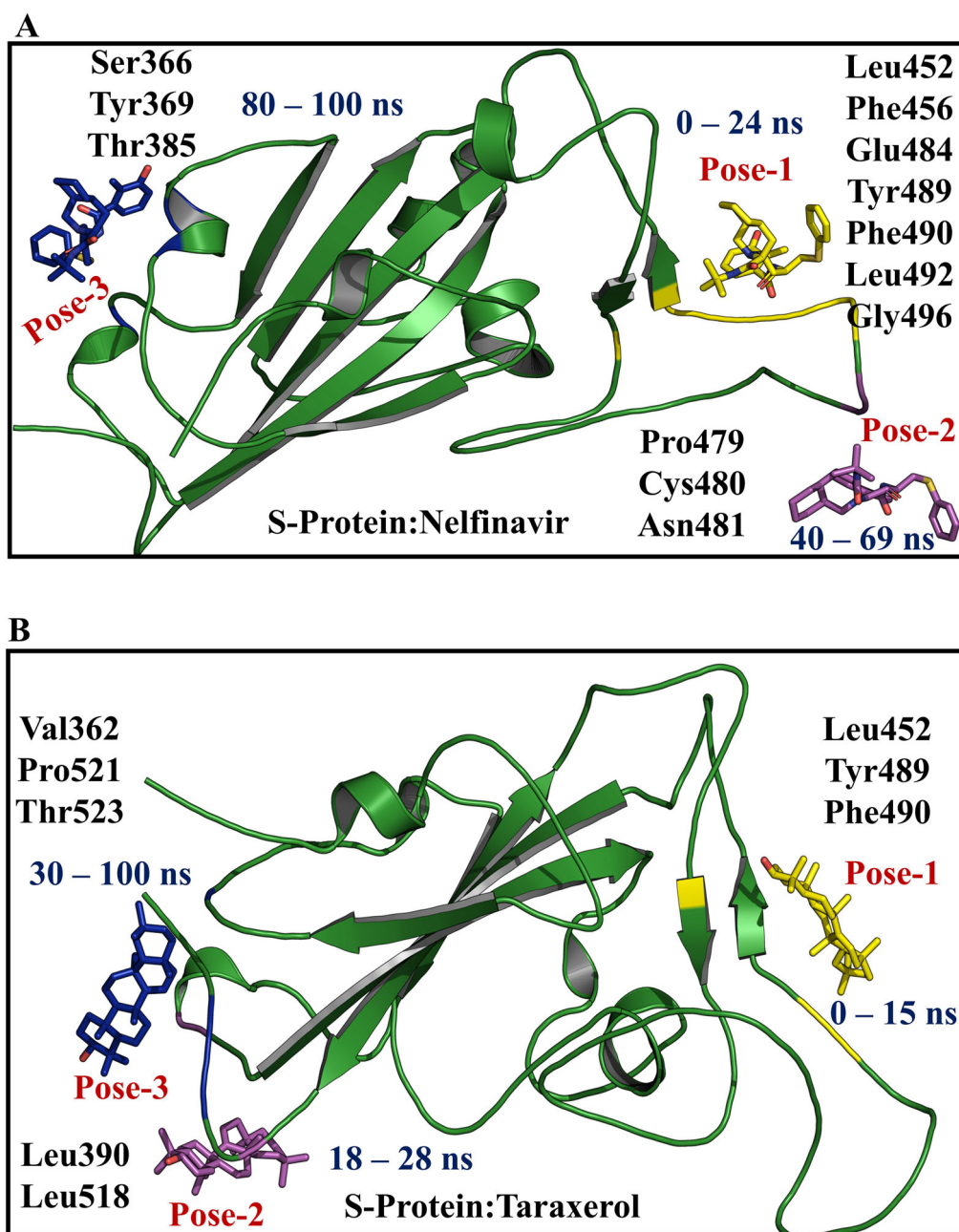


Figure 3. Displacements of nelfinavir and taraxerol during MD simulation with S-protein. (A) Cartoon diagram of S-protein: nelfinavir complex. S-protein is shown in the green cartoon. The three poses of nelfinavir are shown in the stick model with different colors and the major interacting residues of S-protein are marked. (B) Cartoon diagram of S-protein:taraxerol complex. The S-protein and taraxerol are colored and shown as A.

angles, dihedral, electrostatic interactions, Van der Waals interactions, polar and nonpolar solvation energies. Of the 100 ns simulation trajectories, the first 10 ns were excluded for MM-GBSA/MM-PBSA analysis to facilitate compete equilibration of the system set up. A total of 900 snapshots from the MD simulations were used to calculate the free energies using MM-GBSA, and MM-PBSA methods.

3. Results and discussion

3.1. Molecular docking

Molecular docking is a computational approach to predict the binding efficiency, and types of interactions between the

ligand and receptors (Kamath et al., 2015, 2016; Salam et al., 2018). The bioactives from several medicinal plants, which are traditionally known to have various health benefits, were investigated in the present study and compared their BE with the standard drugs. Among the standard drugs, nelfinavir, an anti-retroviral and protease inhibitor, has shown a stronger affinity towards all three targets of SARS-CoV-2 with the BE of -8.3 kcal/mol for M^{Pro} , -6.6 kcal/mol for S-protein and -6.4 kcal/mol for ACE2 (Supporting Information Table S1). Many medicinal plant bioactives have also shown a higher binding affinity towards SARS-CoV-2 targets compared to standard drugs. For example, emblicanin A had BE of -9.3 kcal/mol with M^{Pro} ; rutin had BE of -8.2 kcal/mol with S-protein and echinacin had BE of -7.8 kcal/mol with ACE2

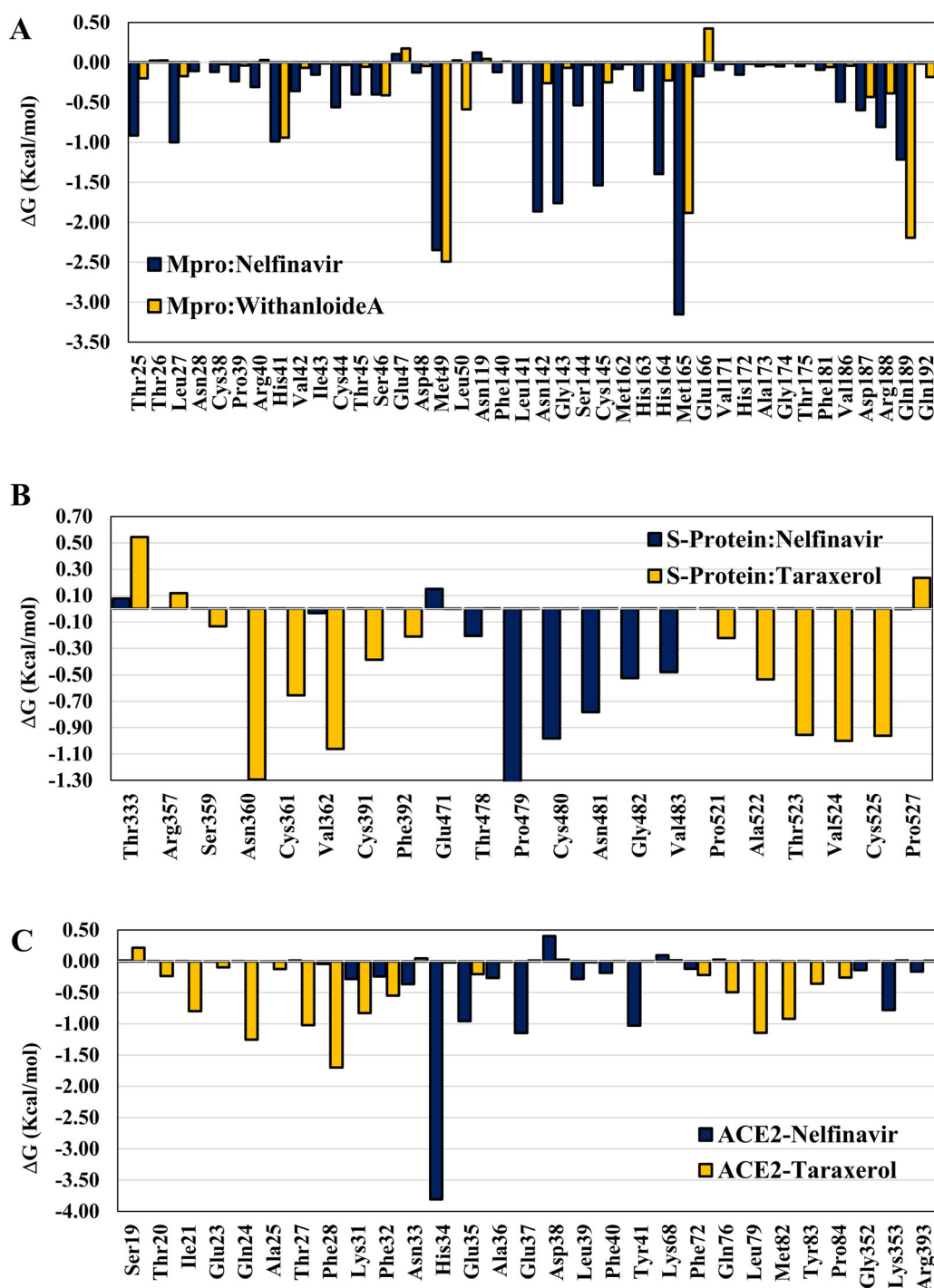


Figure 4. Graphical representation of per residue contribution. (A) Interacting residues of M^{pro} : nelfinavir and M^{pro} : withanolide A are shown as histograms. Amino acids of M^{pro} interacting with nelfinavir and withanolide A are shown on the x-axis and binding energies (kcal/mol) of corresponding residues are shown on the y-axis. (B) S-protein: nelfinavir and S-protein:taraxerol and (C) ACE2-nelfinavir, and ACE2-taraxerol.

(Supporting Information Table S2). Based on the overall BEs of the standard drugs and medicinal plant bioactives, we have set -8.5 kcal/mol, -7.0 kcal/mol and -6.5 kcal/mol as the threshold BEs for M^{pro} , S-protein and ACE2 receptors, respectively. The threshold BEs were used to select the medicinal plant bioactives having a higher binding affinity towards target proteins. We have chosen the bioactive that had shown higher binding affinity against at least two or more potential targets with the minimum fixed threshold BE

for further analysis. Based on these criteria, 15 medicinal plant bioactives, out of sixty screened, were having equal or more binding affinity with more than two targets of SARS-CoV-2, as highlighted in Supporting Information Table S2.

Docking results of the selected medicinal plant bioactives with M^{pro} illustrate that these bioactives have interactions at the catalytic site of proteases, i.e. His41 and Cys145 similar to the standard drugs (Supporting Information Fig. S1-S2). There are 20 amino acids of M^{pro} that frequently make

H-bonds with the medicinal plant bioactives, and their frequencies of interactions are shown in Supporting Information Fig. S3A. Similarly, 25 amino acids of M^{Pro} often make hydrophobic interactions, and their frequencies are shown in Supporting Information Fig. S3B. Similar to standard drugs, bioactives also had a higher binding affinity, and their interactions at the catalytic dyad suggest that the chosen bioactives may also inhibit the activity of M^{Pro} and thereby interfere in the process of viral replication as well as transcription. Among the various selected bioactives, pedunculagin (−8.9 kcal/mol) and echinacin (−8.9 kcal/mol) has shown the highest BE with M^{Pro}. Pedunculagin forms H-bond with Thr26, His41, Ser46, Cys145, His163 as well as it had various non-bonded interactions near the binding pocket of M^{Pro}. Similarly, echinacin forms H-bonds with Thr24, Phe140, His164, Glu166, Arg188, Thr190 and Gln192 in addition, to several non-bonded interactions at the binding pocket of M^{Pro} (Table 1). The interactions of the bioactives at the binding pockets may likely to inhibit the activity of M^{Pro}. In addition, Figure 1(A) shows the common amino acids of M^{Pro} interacting with the standard drug nelfinavir, and bioactive withanolide A as well as taraxerol.

Recently, Jin et al. (2020) solved the structure of M^{Pro} from SARS-CoV-2 (PDB ID: 6LU7), and it is complex with an inhibitor known as N3 (PDB ID: 7BQY; Jin et al., 2020). The N3 inhibitor forms H-bond with amino acids Phe140, Gly143, Cys145, His163, His164, Glu166, Gln189 and Thr190 of M^{Pro} and hydrophobic contacts with Thr26, Leu27, His41, Leu141, Asn142, Met165, Pro168, His172, Arg188 and Gln192 (Jin et al., 2020). Our docking results also mimic the effects of N3, and these interactions identify some more amino acids of M^{Pro}, which may facilitate the drug interactions (Supporting Information Fig. S1 and S2).

During viral transmission, the residues of the receptor-binding motif of S-protein bind with ACE2 receptor hotspots. The receptor-binding motif of S-protein consists of Leu455, Phe486, Gln493 and Ser494 residues, which play a critical role in interacting with the ACE2 receptor (Lan et al., 2020; Yan et al., 2020; Yi et al., 2020; Yuan et al., 2020). In our current study, the selected bioactives from medicinal plants as well as standard drugs have shown interaction towards the key residues of the S-protein receptor-binding motif, as shown in Supporting Information Fig. S4 and S5. The frequency of H-bonds and hydrophobic interactions are also summarized in Supporting Information Fig. S6. Among the bioactive from medicinal plants, withametelin from *Datura* has the highest binding affinity of −8.0 kcal/mol, and it has hydrophobic and non-bonded interactions with Leu452, Phe456, Glu484, Tyr489, Phe490, Leu492, Gln493 and Ser494 of S-protein receptor-binding motif, as shown in Table 1. These interactions at the receptor-binding motif suggest the possibility of bioactives attenuating the spike protein-ACE2 interaction. The common amino acids of the S-protein receptor-binding motif interacting with the standard drug nelfinavir, and bioactives withanolide A, as well as taraxerol, are compared and the results are highlighted in Figure 1(B).

Based on the recent structural and MD studies, many key amino acid residues of the ACE2 receptor are identified in

interacting with its partner proteins (Lan et al., 2020; Veeramachaneni et al., 2020). The human ACE2 receptor contains two hotspot residues Lys31 and Lys353. The S-protein recognizes these hotspots, and their interaction is essential for viral infection. The selected bioactives from the medicinal plants have also shown a higher affinity towards hotspot residues of the ACE2 receptor (Table 1 and Supporting Information Fig. S8). The interactions of the standard drugs and medicinal plant bioactives were also similar towards hotspot residues of the ACE2 receptor as shown in Supporting Information Fig. S7 and S8. Several chosen bioactives had shown a strong interaction with hotspot Lys353 residues, e.g. echinacin (−7.8 kcal/mol) and withametelin (−7.3 kcal/mol). Apart from hotspot Lys353, taraxerol (−7.2 kcal/mol) and quercetin 3-O-robinobioside (−6.2 kcal/mol) have shown strong interactions with the hotspot Lys31. These interactions at the hotspot residues suggest that chosen bioactives can act as ACE2 receptor blockers and can hinder the binding of S-protein.

Overall, the selected medicinal plant bioactives make H-bonds with more than fifteen amino acids of the ACE2 receptor, as shown in Supporting Information Fig. S9A, which are known to interact with its partner proteins frequently. Among them, His34, Glu35, Glu37, Asp38, Ala386, Ala387 and Arg393 show strong and stable interactions with medicinal plant bioactives (Supporting Information Fig. S9A). Besides H-bonding, 29 amino acids of the ACE2 receptor involve in hydrophobic interactions. Among them, Asn33, His34, Glu37, Asp38, Tyr41, Lys353, Gln388, Pro389 and Arg393 residues interact with more than three bioactives (Supporting Information Fig. S9B). The common amino acids of ACE2 receptor interacting with the standard drug nelfinavir, and bioactivities withanolide A, as well as taraxerol, are shown in Figure 1(C). Thus, our docking results revealed the interaction of potential bioactives with key amino acid residues of the SARS-CoV-2 M^{Pro}, S-protein and ACE2 receptor proteins. The bioactives from the selected medicinal plants have shown a stronger affinity with SARS-CoV-2 target proteins. Many of these medicinal plants are well known for their existing anti-viral properties, as outlined in Supporting Information Table S3. Among *Terminalia chebula* possess anti-viral activity against herpes simplex virus-2 and has the efficiency to prevent virus attachment and diffusion into the host cells (Kesharwani et al., 2017).

Similarly, bioactives of porcupine (*Barleria prionitis*) and licorice (*Glycyrrhiza glabra*) have shown a higher binding affinity towards S-protein and ACE-2 receptor. Bioactives from medicinal plant *B. prionitis*, is already known to have potent activity against the Respiratory Syncytial Virus (Chen et al., 1998). *G. glabra* has been known to inhibit the viral replication of SARS-CoV and function as an inhibitor of Human Immunodeficiency Virus 1 (HIV-1; Fiore et al., 2008). Estari et al. have shown an extract of *Phyllanthus emblica* (Amla) exert anti-HIV activity via inhibition of HIV reverse transcriptase activity (Estari et al., 2012). In concurrence, we also found that bioactives of amla had a higher binding affinity with the targets of SARS-CoV-2. Overall, our results suggest that the selected medicinal plant bioactives may

Table 3. Lipinski's Rule of Five (RO5) for standard drugs.

Drugs	Molecular weight (<500 g/mol)	H-bond donor (<5)	H-bond acceptor (<10)	Log P (<5)	Molar refractivity: (40–130)	Violations
Darunavir	547	3	7	4.35	144.45	2
Dexamethasone	392	2	5	4.27	107.78	0
Enalapril	376	2	5	3.15	100.70	0
Favipiravir	157	3	2	-0.40	27.04	0
Losartan	422	2	1	1.63	107.52	0
Nelfinavir	567	3	4	5.77	167.20	3
Olmesartan	446	3	3	1.83	116.22	0
Remdesivir	602	6	10	-	-	3

potentially attenuate the interaction between S-protein and ACE2 receptor as well as inhibit the activity of M^{PRO}. Thus, inhibition of M^{PRO} and attenuation of S-protein-ACE2 interaction may affect replication, maturation and transmission of SARS-CoV-2. Furthermore, by analyzing the additional properties such as druggability and pharmacological features one can gain knowledge about the druggable option of these bioactives.

Further, we determined inhibition constant (K_i) for the bioactives from the medicinal plants and standard drugs. K_i measures the concentration required to produce half-maximum inhibition and 1–40 μM is considered as a preferred range for a hit compound (Naidoo et al., 2020). The K_i calculated for the bioactives from medicinal plants for all three target proteins are summarized in Table 2. In comparison with bioactives, some of the standard drugs such as favipiravir have demonstrated higher K_i values for all three protein targets. Overall, these results suggest that selected medicinal bioactives have a significant binding affinity towards all the protein targets.

3.2. Drug-likeness properties

The drug-likeness property is an essential parameter to find the ability of a compound to become a drug. Based on the Lipinski's rule of five (RO5), we have analyzed the drug-likeness properties of eight standard drugs (Table 3) and fifteen selected medicinal plant bioactives (Table 4). Among them, bioactives from medicinal plants having a maximum of three violations were selected for analyzing other pharmacological features since the selected standard drug Nelfinavir has shown three violations. Seven bioactives (daturaolone, deoxytubulosine, gallotannins taraxerol, tinosporide, withametelin, withanolide A) have qualified the features of drug-likeness with maximum acceptable violations of three, as highlighted in Table 4.

The lipophilicity (LogP) is an essential factor in drug-likeness properties, which influences the absorption rate of the drug molecule in the body. A higher LogP value represents a lower absorption. The standard drugs and medicinal plant bioactives were further screened for Ghose filter rule, Veber rule, Egan rule and Muegge rule, which are also associated with the drug-likeness properties. Most of the standard drugs have qualified all the drug-likeness features, as shown in Supporting Information Table S4.1. In medicinal plant bioactives, tinosporide has qualified all the drug-likeness features, as shown in Supporting Information Table S4.2. All the other

chosen medicinal plant bioactives may have good oral bio-availability and optimal cell permeability as they have low molecular weight and less TPSA value similar to standard drugs. Synthetic accessibility (SA) evaluates the feasibility of the chemical synthesis of the compound. The SA value 1 signifies easy to synthesize, whereas 10 means challenging to synthesize (Ertl & Schuffenhauer, 2009). The SA value of these selected bioactives was in between 4.05 and 6.60, which implies that they can be chemically synthesized with a moderate effort.

3.3. Prediction of ADME/Toxicity

ADME/T analysis is aimed to analyze the absorption, distribution, metabolism, excretion and toxicity of the medicinal plant bioactives *in silico*. The ADME/T results are calculated for the standard drugs and bioactives are represented in Tables 5 and 6, respectively. A desirable compound should have excellent human intestinal absorption (HIA) and Caco-2 cell permeability (Radchenko et al., 2016). Generally, the *in vitro* drug permeability is analyzed using the Caco-2 cell line. We found that most of the chosen medicinal plant bioactives have shown an optimal Caco-2 permeability with higher HIA- and GI-absorptions. In contrast, some of the standard drugs including remdesivir and nelfinavir have not shown an optimal Caco-2 permeability and high GI-absorption. Irrespective of absorption and probable toxicity, a recent double-blind study has shown that the administration of remdesivir improved the recovery of patients who were infected with SARS-CoV-2 and lower respiratory tract infections (Beigel et al., 2020). Advantageously, the selected bioactives not only having comparable BEs but also have better pharmacological distributions over selected standard drugs. Further, we also found that bioactives have the potential to inhibit P-glycoprotein (P-gp) as similar to standard drugs. P-gp is one of the important drug efflux transporters involved in maintaining intracellular drug concentrations (Sève & Dumontet, 2005).

After intestinal absorption, the bioactive molecules circulate into the different parts of the body through blood. Most of the selected bioactives have shown a lesser affinity to bind with plasma protein (PPB) in contrast to some of the standard drugs and, therefore, they are expected to be freely available at the required tissue or organ. After the circulation, the bioactives are metabolized in the liver by the family of the Cytochrome P450 enzymes (Glue & Clement, 1999). Here, few drugs and bioactives functioned as the substrate for these enzymes; consequently, the corresponding CYP450 enzyme might metabolize them.

Table 4. Lipinski's Rule of Five (RO5) for selected bioactives from the medicinal plants.

Bioactive	Molecular weight (<500 g/mol)	H-bond donor (<5)	H-bond acceptor (<10)	Log P (<5)	Molar refractivity: (40–130)	Violations	Meet RO5 criteria
Barlerinoside	930	13	23	5.10	217.67	5	No
Chebularic acid	954	10	27	−0.59	182.03	4	No
Chebulinic acid	956	12	27	0.900	185.99	4	No
Daturaolone	440	1	2	7.48	151.90	2	Yes
Deoxytubulosine	459	1	2	5.22	139.01	2	Yes
Echinacin	578	6	12	2.50	132.60	4	No
Gallotannins	636	11	18	0.94	127.78	3	Yes
Glycyrrhizin	822	6	16	7.50	216.73	5	No
Pedunculagin	784	11	22	−1.78	147.68	4	No
Punigluconin	802	13	23	0.78	156.52	4	No
Quercetin 3-O-robinobioside	610	10	16	1.83	132.33	4	No
Taraxerol	426	1	1	7.82	153.43	2	Yes
Tinosporide	374	0	7	2.39	91.27	0	Yes
Withametelin	436	0	4	5.23	129.10	1	Yes
Withanolide A	470	0	6	5.88	136.95	2	Yes

Bioactives in the bold column were chosen for further analysis based on the minimum acceptable Lipinski's violations.

3.4. Toxicity prediction of bioactives

Toxicity prediction is one major factor in scoring any compound as a drug. The *in silico* toxicological profile of the medicinal plant bioactives was determined by the ProTox-II server and compared with the standard drugs (Drwal et al., 2014). The LD₅₀ values of standard drugs and predictive different organ toxicity are given in Supporting Information Table S5.1. Globally Harmonized System of Classification and Labelling of Chemicals classified different classes of toxicity of orally consumed compounds, described in Supporting Information Table S5.2. Bioactives from medicinal plants shown a range of LD₅₀ values. Daturaolone and taraxerol were non-toxic as their LD₅₀ was 8800 mg/kg, 70,000 mg/kg, respectively. In contrast, withanolide A was falling under class 2 toxicity. Structural modification is one of the new techniques to reduce the toxicity of any compounds. Recently, different chemical strategies such as applying the structural alert in molecules can reduce the toxicity. These structural alerts reduce the toxicity by partial replacement or a full replacement, or by reducing the electronic density or by introducing the structural element involved in metabolism (Limban et al., 2018). The level of toxicity also can be reduced by consuming them as dietary formulations rather than purified compounds or drugs. Therefore, toxicity can be reduced by structural alteration or by chemical strategies. Most of the chosen bioactives did not show any hepatotoxicity, mutagenicity and cytotoxicity.

3.5. Prediction of biological activities

PASS is used to estimate the probable biological activities of drug-like compounds (Filimonov et al., 2014). Different biological activities, including anti-viral activities, were assessed by determining the Pa and Pi values. The PASS analysis of standard drugs and bioactives from the medicinal plants is presented in Supporting Information Table S6.1 and S6.2, respectively. The Pa value towards 1, indicates the ligand is probably 'active', whereas the Pi value implies that the ligand is probably 'inactive'. Approximately seventeen proposed biological activities were determined. The results have shown

that some of the medicinal plant bioactives can act as potent anti-inflammatory and immunosuppressant. However, most of the standard drugs have shown different anti-viral properties, at the same time, some of them also have shown immunostimulatory properties. The chosen bioactives also exert various biological activities, which can act as complementary medicine during the COVID-19 disease.

Similarly, the BAS of the selected medicinal plant bioactives were evaluated for various biological ligands and enzymes. It is known that if the BAS of a ligand is < −0.50, then it is inactive on that target receptors, likewise, if BAS is −0.50 to 0.00, ligands are moderately active, and if BAS is >0.00, then it is biologically active against human receptor and proteins like GPCRs, ion channels, nuclear receptor, proteases and kinases (Mishra et al., 2018). Our results of selected medicinal plant bioactives exhibited biological activities and have a physiological effect. Further, standard drugs were shown to have high activity towards protease inhibition, similarly, the selected medicinal plant bioactives also demonstrated moderate to high activity against protease inhibition, apart from having an activity like enzyme inhibition, and interaction with nuclear and GPCR ligand receptors as shown in Supporting Information Table S7. The protease inhibitory activity of selected medicinal plant bioactives provides further evidence that these bioactives can bind and potentially modulates the main proteases of SARS-CoV-2.

3.6. MD simulation

Unrestrained MD simulations were performed for M^{PRO} with nelfinavir, M^{PRO} with withanolide A, S-protein with nelfinavir, S-protein with taraxerol, ACE2 with nelfinavir and ACE2 with taraxerol complexes, each for 100 ns. In the M^{PRO}-nelfinavir complex, nelfinavir is fairly stable throughout the simulation at the binding pocket (Supporting Information video S1). Similarly, in M^{PRO}-withanolide A complex (Supporting Information video S2), withanolide A molecule is stable and remains inside the pocket. From the RMSD plot, it is evident that the backbone of the M^{PRO} did not converge in both cases. The RMSD of the M^{PRO}-nelfinavir complex is sampling

Table 5. Results of ADME/T-test of the standard drugs.

Absorption Properties	Darunavir	Dexamethasone	Enalapril	Favipiravir	Losartan	Nelfinavir	Olmesartan	Remdesivir
Caco-2 Permeability (Optimal: higher than -5.15 Log unit or -4.70 or -4.80)	Not optimal -5.83 cm/s	Optimal -4.867 cm/s	Not optimal -5.473 cm/s	Optimal -4.466 cm/s	Optimal -5.116 cm/s	Not optimal -5.254 cm/s	Not optimal -5.43 cm/s	Not optimal -6.145 cm/s
Human Intestinal Absorption (HIA) ≥30%: HIA+; <30%: HIA-P-glycoprotein substrate	- (0.426)	++ (0.729)	+ (0.653)	+ (0.542)	++ (0.718)	- (0.3)	+ (0.583)	- (0.301)
P-glycoprotein inhibitor	- (0.495)	+ (0.5)	--- (0.179)	--- (0.011)	++ (0.716)	+ (0.686)	+ (0.511)	--- (0.142)
Bioavailability score	++ (0.858)	- (0.376)	+++ (0.954)	--- (0.042)	++ (0.831)	++ (0.842)	+ (0.665)	++ (0.863)
GI absorption	0.55 Low	0.55 High	0.55 High	0.55 High	0.56 High	0.55 Low	0.56 High	0.17 Low
Distribution Properties								
PPB (Plasma Protein Binding) : 90%	Darunavir Optimal (93.448 %)	Dexamethasone Less (67.738 %)	Enalapril Less (76.383 %)	Favipiravir Very Less (20.55 %)	Losartan Optimal (90.596 %)	Nelfinavir Optimal (94.791 %)	Olmesartan Optimal (91.5 %)	Remdesivir Little less (89.386 %)
Blood-Brain Barrier (BBB)BB ratio >=0.1: BBB+; BB ratio <0.1: BBB-	--- (0.187)	+++ (0.989)	--- (0.043)	+++ (0.996)	--- (0.059)	--- (0.043)	--- (0.034)	--- (0.175)
VD (Volume Distribution) 0.04 ~ 20 L/kg	-1.228 L/kg	-0.036 L/kg	-0.278 L/kg	-0.686 L/kg	-0.111 L/kg	0.234 L/kg	-0.823 L/kg	-1.167 L/kg
Metabolism Properties								
P450 CYP1A2 inhibitor	Darunavir --- (0.041)	Dexamethasone --- (0.023)	Enalapril --- (0.034)	Favipiravir --- (0.075)	Losartan + (0.6)	Nelfinavir --- (0.093)	Olmesartan --- (0.089)	Remdesivir --- (0.138)
P450 CYP1A2 Substrate	- (0.452)	- (0.413)	- (0.378)	+ (0.52)	+ (0.516)	- (0.444)	- (0.44)	- (0.304)
P450 CYP3A4 inhibitor	++ (0.723)	--- (0.246)	--- (0.069)	--- (0.021)	+ (0.636)	+++ (0.907)	+ (0.565)	+ (0.693)
P450 CYP3A4 substrate	+++ (0.916)	+++ (0.946)	+++ (0.817)	--- (0.264)	+++ (0.836)	+++ (0.89)	+ (0.592)	- (0.454)
P450 CYP2C9 inhibitor	+ (0.566)	--- (0.024)	--- (0.048)	--- (0.017)	+++ (0.752)	+ (0.571)	+ (0.634)	+ (0.568)
P450 CYP2C9 substrate	+++ (0.703)	--- (0.022)	--- (0.078)	--- (0.292)	+++ (0.791)	+++ (0.748)	+ (0.605)	- (0.332)
P450 CYP2C19 inhibitor	--- (0.136)	--- (0.089)	--- (0.109)	--- (0.066)	+++ (0.842)	- (0.382)	- (0.473)	- (0.472)
P450 CYP2C19 substrate	- (0.408)	- (0.41)	- (0.407)	--- (0.216)	- (0.492)	+++ (0.766)	- (0.346)	--- (0.238)
P450 CYP2D6 inhibitor	- (0.496)	+ (0.523)	- (0.337)	--- (0.172)	+ (0.562)	- (0.456)	- (0.461)	- (0.385)
P450 CYP2D6 substrate	+ (0.636)	--- (0.009)	--- (0.202)	--- (0.218)	--- (0.195)	+++ (0.856)	--- (0.223)	- (0.331)
Excretion Properties								
T _{1/2} (Half-Life Time; Range: >8 h: high; 3 h < Cl < 8 h: moderate; <3 h: low)	Darunavir Low (1.32 h)	Dexamethasone Low (1.27 h)	Enalapril Low (0.95 h)	Favipiravir Low (0.69 h)	Losartan Low (2.01 h)	Nelfinavir Low (1.58 h)	Olmesartan Low (1.74 h)	Remdesivir Low (1.42 h)
Toxicity								
Properties	Darunavir ++ (0.7)	Dexamethasone ++ (0.7)	Enalapril - (0.427)	Favipiravir - (0.171)	Losartan ++ (0.874)	Nelfinavir ++ (0.764)	Olmesartan ++ (0.743)	Remdesivir + (0.65)
HERG (HERG Blockers)	---	---	---	---	+	---	-	---
AMES (Ames Mutagenicity)	(0.13)	(0.13)	(0.11)	(0.232)	(0.552)	(0.194)	(0.362)	(0.276)
DILI (Drug-Induced Liver Injury)	+++ (0.936)	---	- (0.35)	+++ (0.786)	+++ (0.886)	+ (0.694)	+++ (0.774)	+++ (0.772)

Table 6. Results of ADME/T-test of the selected bioactives from medicinal plants.

Absorption							
Properties	Daturaolone	Deoxytubulosine	Gallotannins	Taraxerol	Tinosporide	Withanolide A	Withametelin
Caco-2 permeability (Optimal: higher than -5.15 Log unit or -4.70 or -4.80)	Optimal -4.715 cm/s	Optimal -5.15 cm/s	Not optimal -6.668 cm/s	Optimal -4.718 cm/s	Optimal -5.017 cm/s	Optimal -5.092 cm/s	Optimal -4.74 cm/s
Human Intestinal Absorption (HIA) $\geq 30\%$: HIA+; $<30\%$: HIA-	+++ (0.904)	++ (0.706)	--- (0.177)	+++ (0.915)	+ (0.61)	+ (0.611)	+ (0.679)
P-glycoprotein substrate	--- (0.036)	+++ (0.925)	--- (0.005)	--- (0.042)	--- (0.167)	--- (0.087)	--- (0.097)
P-glycoprotein inhibitor	--- (0.299)	++ (0.72)	--- (0.123)	--- (0.263)	- (0.354)	++ (0.795)	++ (0.765)
Bioavailability score	0.55	0.55	0.17	0.55	0.55	0.55	0.55
GI absorption	Low	High	Low	Low	High	High	High
Distribution							
Properties	Daturaolone	Deoxytubulosine	Gallotannins	Taraxerol	Tinosporide	Withanolide A	Withametelin
PPB (Plasma Protein Binding): 90%	Less (80.905 %)	Less (86.055 %)	Less (71.82%)	Less (80.527 %)	Less (64.597 %)	Less (88.199 %)	Less (84.515 %)
Blood-Brain Barrier (BBB)BB ratio ≥ 0.1 : BBB+; BB ratio <0.1 : BBB-	++ (0.867)	- (0.337)	- (0.42)	+++ (0.951)	+ (0.643)	++ (0.705)	++ (0.892)
VD (Volume Distribution) 0.04 ~ 20 L/kg	-0.012 L/kg	1.251 L/kg	-1.291 L/kg	0.283 L/kg	-0.154 L/kg	-0.107 L/kg	-0.208 L/kg
Metabolism							
Properties	Daturaolone	Deoxytubulosine	Gallotannins	Taraxerol	Tinosporide	Withanolide A	Withametelin
P450 CYP1A2 inhibitor	--- (0.037)	--- (0.08)	--- (0.038)	--- (0.035)	--- (0.062)	--- (0.052)	--- (0.051)
P450 CYP1A2 Substrate	- (0.352)	+ (0.564)	--- (0.226)	- (0.372)	- (0.468)	- (0.463)	+ (0.566)
P450 CYP3A4 inhibitor	--- (0.076)	--- (0.272)	--- (0.074)	--- (0.046)	--- (0.283)	+ (0.511)	- (0.35)
P450 CYP3A4 substrate	+ (0.651)	+ (0.652)	--- (0.202)	+ (0.59)	+ (0.668)	+ (0.693)	+ (0.642)
P450 CYP2C9 inhibitor	--- (0.057)	--- (0.099)	--- (0.144)	--- (0.028)	--- (0.179)	- (0.31)	--- (0.277)
P450 CYP2C9 substrate	- (0.361)	- (0.328)	- (0.353)	--- (0.274)	--- (0.287)	--- (0.273)	- (0.3)
P450 CYP2C19 inhibitor	--- (0.118)	--- (0.17)	--- (0.042)	--- (0.134)	--- (0.103)	--- (0.165)	--- (0.225)
P450 CYP2C19 substrate	- (0.426)	+ (0.56)	--- (0.208)	- (0.406)	+ (0.61)	- (0.472)	+ (0.687)
P450 CYP2D6 inhibitor	--- (0.226)	++ (0.702)	- (0.361)	- (0.318)	- (0.349)	--- (0.297)	--- (0.28)
P450 CYP2D6 substrate	- (0.305)	++ (0.799)	- (0.355)	- (0.36)	--- (0.23)	--- (0.298)	- (0.346)
Excretion							
Properties	Daturaolone	Deoxytubulosine	Gallotannins	Taraxerol	Tinosporide	Withanolide A	Withametelin
T 1/2 (Half Life Time; >8 h: high; $3\text{h} < \text{Cl} < 8$ h: moderate; <3 h: low)	Low (1.67 h)	Low (1.79 h)	Low (1.86 h)	Low (1.88 h)	Low (1.19 h)	Low (1.6 h)	Low (1.91 h)
Toxicity							
Properties	Daturaolone	Deoxytubulosine	Gallotannins	Taraxerol	Tinosporide	Withanolide A	Withametelin
hERG (hERG Blockers)	- (0.455)	++ (0.844)	+ (0.632)	- (0.468)	--- (0.188)	- (0.449)	+ (0.519)
AMES (Ames Mutagenicity)	--- (0.07)	- (0.33)	- (0.354)	--- (0.036)	--- (0.266)	--- (0.29)	--- (0.196)
DILI (Drug Induced Liver Injury)	- (0.468)	--- (0.224)	++ (0.744)	--- (0.214)	- (0.368)	--- (0.278)	- (0.446)

higher values after 70 ns, whereas in M^{PRO}-withanolide A complex, the RMSD is reaching a maximum of around 40 ns, then is stable at 4 Å minimum and gain the stability (Figure 2(A)). Since the stability of ligand binding at its pocket is evident from the simulation videos, the fluctuations in the RMSD are likely due to changes in the regions other than its catalytic site; hence, these do not alter our main discussion points.

The S-protein-nelfinavir complex (Supporting Information video S3) showed quite interesting binding patterns during the simulations. The nelfinavir molecule is initially bound at the cavity formed by the amino acids Leu452-Phe456, and Glu484-Gly496 of S-protein, and it retained its pose up to

24 ns. It then dissociates from the binding pocket, floats free among the bulk solvent and binds again to the protein between 40 and 69 ns. It dissociates from the second position too and it finally moves to a third pose at a site diametrically across the molecule from the starting pocket and stays stable from 80 to 100 ns (Figure 3(A)). The S-protein-taraxerol complex, taraxerol moves away from its initial binding pose taking up a second position after 15 ns, reaches its final position around 30 ns and remains stable during the rest of the simulation (Figure 3(B)). The recent X-ray crystallographic structural studies of S-protein with monoclonal antibody CR3022 revealed that the CR3022 binds the same site where the nelfinavir and taraxerol move to the final position (third

Table 7. MM-GBSA and MM-PBSA calculations of binding energy for six selected complex molecules.

Analysis type	Energy Component	M ^{Pro} -Nelfinavir	M ^{Pro} -Withanolide A	S-protein-Nelfinavir	S-protein-Taraxerol	ACE2-Nelfinavir	ACE2-Taraxerol
		DeltaG (kcal/mol)					
GBSA	VDWAAL	-55.9 (5.4)	-35.3 (4.7)	-14.8 (8.7)	-22.9 (5.1)	-33.7 (4.7)	-30.1 (4.4)
	EEL	-17.7 (6.4)	-12.0 (6.8)	-9.3 (8.1)	-0.8 (2.0)	-32.5 (7.7)	-1.4 (3.4)
	EGB	28.8 (5.3)	23.7 (5.2)	14.2 (9.2)	7.9 (2.1)	44.2 (6.7)	8.8 (2.8)
	ESURF	-6.8 (0.6)	-4.4 (0.5)	-1.9 (1.1)	-2.5 (0.5)	-4.3 (0.6)	3.6 (0.5)
	Total	-51.7 (6.3)	-27.9 (5.4)	-11.8 (7.8)	-18.2 (4.5)	-26.3 (4.4)	-26.2 (4.2)
PBSA	VDWAAL	-55.9 (5.4)	-35.3 (4.7)	-14.8 (8.7)	-22.9 (5.1)	-33.7 (4.7)	-30.1 (4.4)
	EEL	-17.7 (6.4)	-12.0 (6.8)	-9.3 (8.1)	-0.8 (2.0)	-32.5 (7.7)	-1.4 (3.4)
	EPB	39.1 (6.0)	24.9 (6.6)	13.0 (9.1)	6.3 (2.4)	46.3 (8.3)	7.9 (2.9)
	ENPOLAR	-39.0 (3.0)	-25.0 (3.1)	-11.2 (6.8)	-15.2 (3.0)	-24.8 (3.0)	-21.8 (2.8)
	Total	-3.1 (6.4)	-0.7 (4.4)	-2.4 (4.0)	-4.2 (3.0)	-2.4 (4.9)	-7.3 (3.2)

pose; Huo et al., 2020). The authors postulated that the CR3022 binding to amino acids 369–392, and 427–430 of S-protein, leads to neutralization mechanism by destroying the prefusion spike conformation. Figure 2(A) plot shows that S-protein – nelfinavir or taraxerol complex structures remain stable with their RMSD mostly staying below 2 Å from their starting respective structures.

In the ACE2-nelfinavir complex (Supporting Information video S5), the nelfinavir is stable in the entire study. In the ACE2-taraxerol complex study (Supporting Information video S6), the taraxerol molecule is flipping from the docked position in early stages around 1.7 ns, then become stable and change its orientation around 84 ns simulation. The RMSD plot of ACE2-nelfinavir and ACE2-taraxerol shows that the overall structure of ACE2-nelfinavir is relatively more stable than the ACE2-taraxerol complex structure during the course of the MD simulation (Figure 2(A)).

3.7. MM-GBSA and MM-PBSA calculations

Binding free energies calculated using MM-GBSA and MM-PBSA methods are shown in Table 7 for all the six complex molecules. Initial 10 ns frames or omitted for equilibration, and a total of 900 frames out of the remaining 90 ns simulations were used to obtain the free energy all the systems. In terms of MM-GBSA M^{Pro}-nelfinavir showed the highest energy (-51.7 kcal/mol). M^{Pro}-withanolide A (-27.9 kcal/mol), ACE2-nelfinavir (-26.3 kcal/mol) and ACE2-taraxerol (-26.2 kcal/mol) showed similar energies. In terms of MM-PBSA, ACE2-taraxerol (-7.3 kcal/mol) showed the highest affinity than other complex molecules. The BE versus time graphs (Figure 2(B–D)) is drawn for all the complexes. In terms of M^{Pro} complexes, both nelfinavir and taraxerol showed similar energies, whereas the ACE2, and S-protein complexes, taraxerol shows better binding energies than the standard drug nelfinavir. It should be noted that taraxerol has only one hydroxyl and seven methyl groups attached to the pentacyclic triterpenoid. The taraxerol possess anti-tumor (Hong et al., 2016), and anti-inflammatory (Yao et al., 2013) activities, and one of the abundantly available medicinal phytochemicals that can be extracted from more than 50 medicinal plants (Sharma & Zafar, 2015).

In addition to that, we analyzed the contribution of each residue to the BE using the decomposition tool present in the AMBER: MM-GBSA method. Forty residues of M^{Pro} has shown significant interaction with nelfinavir and/or

withanolide A (Figure 4(A)). Among those His41, Met49, Met165 and Gln189 are common residues that showed favorable binding energies with the medicinal phytochemical compounds. Apart from that Thr25, Leu29, Asn142, Gly143, Cys145, His164 and Gln189 of M^{Pro} showed good interaction with nelfinavir, and Ser46, Leu50, Asp187, Arg188, Gln189, Asn142 and Cys145 of M^{Pro} showed higher binding energies with withanolide A. Recent studies on M^{Pro} with bioactive molecules from the tea plant, showed similar interactions (Bhardwaj et al., 2020). Among those residues, His41 and Cys145 form a catalytic dyad located at the interface between domains I and II, and most of the remaining residues are involved in substrate binding and dimerization (Goyal & Goyal, 2020). Thr478, Pro479, Cys480, Asn481, Gly482 and Val483 of S-protein show better binding energies with nelfinavir, whereas the taraxerol have significant binding energies at three different positions Ser359-Val363, Cys391-Phe392 and Pro521-Cys525 (Figure 4(B)). Recent mutagenesis studies identified that Arg439, Lys452, Leu455, Ala475, Glu484, Phe486, Gln493, Gln498, Pro499 and Asn501 of S-protein play a major role in human ACE2 binding (Yi et al., 2020), and these residues are closely matching with our results. It is also interesting to note that the taraxerol is having reasonable binding energies with three cysteine residues (Cys361, Cys391 and Cys525), which play role in stabilizing the secondary structure of S-protein (Lan et al., 2020). The ACE2 complexes, His34 and Phe28 of ACE2 are the two major amino acids that have a higher binding affinity with nelfinavir and taraxerol, respectively (Figure 4(C)). Interestingly His34 of ACE2 is the common residues interacting with both SARS-Cov S-protein and SARS-Cov-2 S-protein (Lan et al., 2020).

The hydrogen bonds formed during the simulation time in all the six complex molecules were calculated using CPPTraj (Roe & Cheatham, 2013). The amino acids His164, Gly143 (M^{Pro}-nelfinavir), His164, Gln189 (M^{Pro}-withanolide A), Glu484, Cys480 (S-protein-nelfinavir), Gly381, Glu484 (S-protein-taraxerol), His34, Asp30 (ACE2-nelfinavir) and Gln76, Glu75 (ACE2-taraxerol) are the top two residues interacting with the respective ligands.

4. Conclusion

The infectious pandemic COVID-19 has emerged as a massive threat to humankind. The main challenges are to control the spread of the disease, developing immunity as the

preventive as well as prophylactic, and discovering therapeutics in a feasible time. Nature has always blessed us with plentiful remedies like herbs and medicinal plants for numerous ailments. Therefore, the virtual screening based on molecular docking was executed to identify potential bioactives from medicinal plants as effective inhibitors of M^{pro}, S-protein and ACE2. We found many bioactives from the medicinal plants have shown either comparable or better binding affinity with targets of SARS-CoV-2 with desirable pharmacological properties over the standard drugs. Further, we also observed that the selected bioactives have better intestinal and GI absorptions and lower toxicity than the standard drugs used. Therefore, these selected bioactives may further be developed as pharmacological inhibitors against SARS-CoV-2 target proteins involved in viral replication, propagation and transmission. Among them, taraxerol from *Clerodendrum* has shown potential anti-viral activities with desirable pharmacological features (Sharma & Zafar, 2015; Verma & Baranwal, 1983). Further, withanolide A from *Withania somnifera* has shown the highest binding affinity with S-protein and ACE-2 receptor. The active constituents of ayurvedic herb *W. somnifera* have shown promising anti-influenza properties by targeting neuraminidase of H1N1 influenza (Cai et al., 2015). AYUSH Ministry of Health, India, has further recommended the use of the aqueous extract of this plant as a preventive and prophylactic for treating COVID-19. Withametelin, from the *Datura innoxia* plant, has shown a better binding affinity against M^{pro}, S-protein and ACE2. However, the pharmacological analysis revealed its toxicity to health. Instead, daturaolone, another compound from *D. innoxia*, have shown lower toxicity and higher HIA with potent anti-viral and anti-inflammatory activities. Overall, the selected medicinal plant bioactives can be further developed and assessed as phytoformulations against SARS-CoV-2 infection.

Acknowledgments

CSIR-CFTRI for the support and infrastructure facility. We thank Dr. Laskowski (The European Bioinformatics Institute (EMBL-EBI, Cambridgeshire, UK) for his valuable suggestions and providing customized LigPlot program. We thank Professor David A. Case (Rutgers University, NJ, USA) for providing access to the latest AMBER20 software.

Disclosure statement

No potential conflict of interest was reported by the authors.

Funding

PM acknowledges senior research fellowships from UGC, Government of India, and JN from DBT, Government of India. AAAS acknowledges the research grant provided by a MAHE intramural grant [grant no. MAHE/DREG/PhD/IMF/2019]. ST acknowledges the institutional grant to IBAB from the Department of IT, BT, Science and Technology, the Government of Karnataka. IBAB is also supported by DST-FIST vide sanction no SR/FST/LSI-536/2012.

References

- Andersen, K. G., Rambaut, A., Lipkin, W. I., Holmes, E. C., & Garry, R. F. (2020). The proximal origin of SARS-CoV-2. *Nature Medicine*, 26(4), 450–452. <https://doi.org/10.1038/s41591-020-0820-9>
- Beigel, J. H., Tomashek, K. M., Dodd, L. E., Mehta, A. K., Zingman, B. S., Kalil, A. C., Hohmann, E., Chu, H. Y., Luetkemeyer, A., Kline, S., Lopez de Castilla, D., Finberg, R. W., Dierberg, K., Tapson, V., Hsieh, L., Patterson, T. F., Paredes, R., Sweeney, D. A., Short, W. R., ... Lane, H. C. (2020). Remdesivir for the treatment of Covid-19 — Preliminary report. *New England Journal of Medicine*, NEJMoa2007. PMID: 32445440. <https://doi.org/10.1056/nejmoa2007764>
- Bhardwaj, V. K., Singh, R., Sharma, J., Rajendran, V., Purohit, R., & Kumar, S. (2020). Identification of bioactive molecules from tea plant as SARS-CoV-2 main protease inhibitors. *Journal of Biomolecular Structure and Dynamics*. <https://doi.org/10.1080/07391102.2020.1766572>
- Bonow, R. O., Fonarow, G. C., O'Gara, P. T., & Yancy, C. W. (2020). Association of coronavirus disease 2019 (COVID-19) with myocardial injury and mortality. *JAMA Cardiology*, 5(7), 751–753. <https://doi.org/10.1001/jamacardio.2020.1105>
- Cai, Z., Zhang, G., Tang, B., Liu, Y., Fu, X., & Zhang, X. (2015). Promising anti-influenza properties of active constituent of *Withania somnifera* Ayurvedic herb in targeting neuraminidase of H1N1 influenza: Computational study. *Cell Biochemistry and Biophysics*, 72(3), 727–739. <https://doi.org/10.1007/s12013-015-0524-9>
- Case, D. A., Belfon, K., Ben-Shalom, I. Y., Brozell, S. R., Cerutti, D. S., Cheatham, III, T. E., Cruzeiro, V. W. D., Darden, T. A., Duke, R. E., Giambasu, G., Gilson, M. K., Gohlke, H., Goetz, A. W., Harris, R., Izadi, S., Izmailov, S. A., Kasavajhala, K., Kovalenko, A., Krasny, R., ... Kollman, P. A. (2020). AMBER 2020. University of California.
- Chen, J. L., Blanc, P., Stoddart, C. A., Bogan, M., Rozhon, E. J., Parkinson, N., Ye, Z., Cooper, R., Balick, M., Nanakorn, W., & Kernan, M. R. (1998). New iridoids from the medicinal plant *Barleria prionitis* with potent activity against respiratory syncytial virus. *Journal of Natural Products*, 61(10), 1295–1297. <https://doi.org/10.1021/np980086y>
- Cornélio Favarin, D., Robison De Oliveira, J., Jose Freire De Oliveira, C., & De Paula Rogerio, A. (2013). Potential effects of medicinal plants and secondary metabolites on acute lung injury. *BioMed Research International*, 2013, 576479. <https://doi.org/10.1155/2013/576479>
- Daina, A., Michielin, O., & Zoete, V. (2017). SwissADME: A free web tool to evaluate pharmacokinetics, drug-likeness and medicinal chemistry friendliness of small molecules. *Scientific Reports*, 7, 42717. <https://doi.org/10.1038/srep42717>
- Dong, J., Wang, N. N., Yao, Z. J., Zhang, L., Cheng, Y., Ouyang, D., Lu, A. P., & Cao, D. S. (2018). Admetlab: A platform for systematic ADMET evaluation based on a comprehensively collected ADMET database. *Journal of Cheminformatics*, 10(1), 29. <https://doi.org/10.1186/s13321-018-0283-x>
- Drwal, M. N., Banerjee, P., Dunkel, M., Wettig, M. R., & Preissner, R. (2014). ProTox: A web server for the in silico prediction of rodent oral toxicity. *Nucleic Acids Research*, 42(Web Server issue), W53–W58. <https://doi.org/10.1093/nar/gku401>
- Ertl, P., & Schuffenhauer, A. (2009). Estimation of synthetic accessibility score of drug-like molecules based on molecular complexity and fragment contributions. *Journal of Cheminformatics*, 1(1), 8. <https://doi.org/10.1186/1758-2946-1-8>
- Estari, M., Venkanna, L., Sriprya, D., & Lalitha, R. (2012). Human immunodeficiency virus (HIV-1) reverse transcriptase inhibitory activity of phyllanthus emblica plant extract. *Biology and Medicine*, 4(4), 178. <https://doi.org/10.4172/0974-8369.1000175>
- Filimonov, D. A., Lagunin, A. A., Glorizova, T. A., Rudik, A. V., Druzhilovskii, D. S., Pogodin, P. V., & Poroikov, V. V. (2014). Prediction of the biological activity spectra of organic compounds using the pass online web resource. *Chemistry of Heterocyclic Compounds*, 50(3), 444–457. <https://doi.org/10.1007/s10593-014-1496-1>
- Fiore, C., Eisenhut, M., Krausse, R., Ragazzi, E., Pellati, D., Armanini, D., & Bielenberg, J. (2008). Antiviral effects of *Glycyrrhiza* species. *Phytotherapy Research*, 22(2), 141–148. <https://doi.org/10.1002/ptr.2295>

- Ganjhu, R. K., Mudgal, P. P., Maity, H., Dowarha, D., Devadiga, S., Nag, S., & Arunkumar, G. (2015). Herbal plants and plant preparations as remedial approach for viral diseases. *Virusdisease*, 26(4), 225–236. <https://doi.org/10.1007/s13337-015-0276-6>
- Glue, P., & Clement, R. P. (1999). Cytochrome P450 enzymes and drug metabolism - Basic concepts and methods of assessment. *Cellular and Molecular Neurobiology*, 19(3), 309–323. <https://doi.org/1006993631057>
- Goyal, B., & Goyal, D. (2020). Targeting the dimerization of the main protease of coronaviruses: A potential broad-spectrum therapeutic strategy. *ACS Combinatorial Science*, 22(6), 297–305. <https://doi.org/10.1021/acscombsci.0c00058>
- Hepcy Kalarani, D., Dinakar, A., & Senthilkumar, N. (2012). Antidiabetic, analgesic and anti-inflammatory activity of aqueous extracts of stem and leaves of *Alangium salvifolium* and *Pavonia zeylanica*. *International Journal of Drug Development and Research*, 4, 298–306.
- Hong, J. F., Song, Y. F., Liu, Z., Zheng, Z. C., Chen, H. J., & Wang, S. S. (2016). Anticancer activity of taraxerol acetate in human glioblastoma cells and a mouse xenograft model via induction of autophagy and apoptotic cell death, cell cycle arrest and inhibition of cell migration. *Molecular Medicine Reports*, 13(6), 4541–4548. <https://doi.org/10.3892/mmr.2016.5105>
- Huo, J., Zhao, Y., Ren, J., Zhou, D., Duyvesteyn, H. M. E., Ginn, H. M., Carriego, L., Malinauskas, T., Ruza, R. R., Shah, P. N. M., Tan, T. K., Rijal, P., Coombes, N., Bewley, K. R., Tree, J. A., Radecke, J., Paterson, N. G., Supasa, P., Mongkolsapaya, J., ... Stuart, D. I. (2020). Neutralization of SARS-CoV-2 by destruction of the prefusion spike. *Cell Host & Microbe*, 28(3), 445–454.e6. <https://doi.org/10.1016/j.chom.2020.06.010>
- Jin, Z., Du, X., Xu, Y., Deng, Y., Liu, M., Zhao, Y., Zhang, B., Li, X., Zhang, L., Peng, C., Duan, Y., Yu, J., Wang, L., Yang, K., Liu, F., Jiang, R., Yang, X., You, T., Liu, X., ... Yang, H. (2020). Structure of Mpro from SARS-CoV-2 and discovery of its inhibitors. *Nature*, 582(7811), 289–293. <https://doi.org/10.1038/s41586-020-2223-y>
- Kamath, P. R., Sunil, D., & Ajees, A. A. (2016). Synthesis of indole–quinoline–oxadiazoles: Their anticancer potential and computational tubulin binding studies. *Research on Chemical Intermediates*, 42(6), 5899–5914. <https://doi.org/10.1007/s11164-015-2412-8>
- Kamath, P. R., Sunil, D., Ajees, A. A., Pai, K. S. R., & Das, S. (2015). Some new indole-coumarin hybrids; Synthesis, anticancer and Bcl-2 docking studies. *Bioorganic Chemistry*, 63, 101–109. <https://doi.org/10.1016/j.bioorg.2015.10.001>
- Kesharwani, A., Polachira, S. K., Nair, R., Agarwal, A., Mishra, N. N., & Gupta, S. K. (2017). Anti-HSV-2 activity of *Terminalia chebula* Retz extract and its constituents, chebulagic and chebulinic acids. *BMC Complementary and Alternative Medicine*, 17(1), 110. <https://doi.org/10.1186/s12906-017-1620-8>
- Kim, S., Chen, J., Cheng, T., Gindulyte, A., He, J., He, S., Li, Q., Shoemaker, B. A., Thiessen, P. A., Yu, B., Zaslavsky, L., Zhang, J., & Bolton, E. E. (2019). PubChem 2019 update: Improved access to chemical data. *Nucleic Acids Research*, 47(D1), D1102–D1109. <https://doi.org/10.1093/nar/gky1033>
- Lan, J., Ge, J., Yu, J., Shan, S., Zhou, H., Fan, S., Zhang, Q., Shi, X., Wang, Q., Zhang, L., & Wang, X. (2020). Structure of the SARS-CoV-2 spike receptor-binding domain bound to the ACE2 receptor. *Nature*, 581(7807), 215–220. <https://doi.org/10.1038/s41586-020-2180-5>
- Laskowski, R. A., & Swindells, M. B. (2011). LigPlot+: Multiple ligand-protein interaction diagrams for drug discovery. *Journal of Chemical Information and Modeling*, 51(10), 2778–2786. <https://doi.org/10.1021/ci200227u>
- Limban, C., Nuță, D. C., Chiriță, C., Negreș, S., Arsene, A. L., Goumenou, M., Karakitsios, S. P., Tsatsakis, A. M., & Sarigiannis, D. A. (2018). The use of structural alerts to avoid the toxicity of pharmaceuticals. *Toxicology Reports*, 5, 943–953. <https://doi.org/10.1016/j.toxrep.2018.08.017>
- Liperoti, R., Vetrano, D. L., Bernabei, R., & Onder, G. (2017). Herbal medications in cardiovascular medicine. *Journal of the American College of Cardiology*, 69(9), 1188–1199. <https://doi.org/10.1016/j.jacc.2016.11.078>
- Lipinski, C. A. (2004). Lead- and drug-like compounds: The rule-of-five revolution. *Drug Discovery Today: Technologies*, 1(4), 337–341. <https://doi.org/10.1016/j.ddtec.2004.11.007>
- MarvinSketch. (n.d.). MarvinSketch was used to convert chemical structures from 2D to 3D. ChemAxon. <https://www.chemaxon.com>.
- Merad, M., & Martin, J. C. (2020). Pathological inflammation in patients with COVID-19: A key role for monocytes and macrophages. *Nature Reviews: Immunology*, 20(6), 355–362. <https://doi.org/10.1038/s41577-020-0331-4>
- Mishra, A., Dixit, S., Ratan, V., Srivastava, M., Trivedi, S., & Srivastava, Y. K. (2018). Identification and in silico screening of biologically active secondary metabolites isolated from *Trichoderma harzianum*. *Annals of Phytomedicine: An International Journal*, 7(1), 78–86. <https://doi.org/10.21276/ap.2018.7.1.9>
- Morris, G. M., Huey, R., Lindstrom, W., Scanner, M. F., Belew, R. S., Goodsell, D. S., & Olson, A. J. (2009). AutoDock4 and AutoDockTools4: Automated docking with selective receptor flexibility. *Journal of Computational Chemistry*, 30(16), 2785–2791. <https://doi.org/10.1002/jcc.21256>
- Mukhtar, M., Arshad, M., Ahmad, M., Pomerantz, R. J., Wigdahl, B., & Parveen, Z. (2008). Antiviral potentials of medicinal plants. *Virus Research*, 131(2), 111–120. <https://doi.org/10.1016/j.virusres.2007.09.008>
- Nagarkar, B., Nirmal, P., Narkhede, A., Kuvalekar, A., Kulkarni, O., Harsulkar, A., & Jagtap, S. (2013). Comparative evaluation of anti-inflammatory potential of medicinally important plants. *International Journal of Pharmacy and Pharmaceutical Sciences*, 5, 239–243.
- Naidoo, D., Roy, A., Kar, P., Mutanda, T., & Anandraj, A. (2020). Cyanobacterial metabolites as promising drug leads against the Mpro and PLpro of SARS-CoV-2: An in silico analysis. *Journal of Biomolecular Structure and Dynamics*, 1–13. <https://doi.org/10.1080/07391102.2020.1794972>
- O'Boyle, N. M., Banck, M., James, C. A., Morley, C., Vandermeersch, T., & Hutchison, G. R. (2011). Open Babel: An open chemical toolbox. *Journal of Cheminformatics*, 3(1), 33. <https://doi.org/10.1186/1758-2946-3-33>
- Onawole, A. T., Kolapo, T. U., Sulaiman, K. O., & Adegoke, R. O. (2018). Structure based virtual screening of the Ebola virus trimeric glycoprotein using consensus scoring. *Computational Biology and Chemistry*, 72, 170–180. <https://doi.org/10.1016/j.compbiolchem.2017.11.006>
- Pruthvish, R., & Gopinatha, R. P. (2018). Antiviral prospective of *Tinospora cordifolia* on HSV-1. *International Journal of Current Microbiology and Applied Sciences*, 7(1), 3617–3624. <https://doi.org/10.20546/ijcmas.2018.701.425>
- Radchenko, E. V., Dyabina, A. S., Palyulin, V. A., & Zefirov, N. S. (2016). Prediction of human intestinal absorption of drug compounds. *Russian Chemical Bulletin*, 65(2), 576–580. <https://doi.org/10.1007/s11172-016-1340-0>
- Rodríguez-Morales, A. J., MacGregor, K., Kanagarajah, S., Patel, D., & Schlagenhauf, P. (2020). Going global - Travel and the 2019 novel coronavirus. *Travel Medicine and Infectious Disease*, 33, 101578. <https://doi.org/10.1016/j.tmaid.2020.101578>
- Roe, D. R., & Cheatham, T. E. (2013). PTRAJ and CPPTRAJ: Software for processing and analysis of molecular dynamics trajectory data. *Journal of Chemical Theory and Computation*, 9(7), 3084–3095. <https://doi.org/10.1021/ct400341p>
- Roy, S., Mukherjee, S., Pawar, S., & Chowdhary, A. (2016). Evaluation of in vitro antiviral activity of *Datura metel* Linn. against rabies virus. *Pharmacognosy Research*, 8(4), 265–269. <https://doi.org/10.4103/0974-8490.188874>
- Salam, A. A. A., Nayek, U., & Sunil, D. (2018). Homology modeling and docking studies of Bcl-2 and Bcl-xL with small molecule inhibitors: Identification and functional studies. *Current Topics in Medicinal Chemistry*, 18(31), 2633–2663. <https://doi.org/10.2174/1568026619666190119144819>
- Sève, P., & Dumontet, C. (2005). Chemoresistance in non-small cell lung cancer. *Current Medicinal Chemistry. Anti-Cancer Agents*, 5(1), 73–88. <https://doi.org/10.2174/1568011053352604>
- Shahidul Alam, M., Quader, M. A., & Rashid, M. A. (2000). HIV-inhibitory diterpenoid from *Anisomeles indica*. *Fitoterapia*, 71(5), 574–576. [https://doi.org/10.1016/S0367-326X\(00\)00197-0](https://doi.org/10.1016/S0367-326X(00)00197-0)
- Shang, J., Ye, G., Shi, K., Wan, Y., Luo, C., Aihara, H., Geng, Q., Auerbach, A., & Li, F. (2020). Structural basis of receptor recognition by SARS-

- CoV-2. *Nature*, 581(7807), 221–224. <https://doi.org/10.1038/s41586-020-2179-y>
- Sharma, K., & Zafar, R. (2015). Occurrence of taraxerol and taraxasterol in medicinal plants. *Pharmacognosy Reviews*, 9(17), 19. <https://doi.org/10.4103/0973-7847.156317>
- Towler, P., Staker, B., Prasad, S. G., Menon, S., Tang, J., Parsons, T., Ryan, D., Fisher, M., Williams, D., Dales, N. A., Patane, M. A., & Pantoliano, M. W. (2004). ACE2 X-ray structures reveal a large hinge-bending motion important for inhibitor binding and catalysis. *The Journal of Biological Chemistry*, 279(17), 17996–18007. <https://doi.org/10.1074/jbc.M311191200>
- Trott, O., & Olson, A. J. (2010). AutoDock Vina: Improving the speed and accuracy of docking with a new scoring function, efficient optimization, and multithreading. *Journal of Computational Chemistry*, 31(2), 455–461. <https://doi.org/10.1002/jcc.21334>
- Veeramachaneni, G. K., Thunuguntla, V. B. S. C., Bobbillapati, J., & Bondili, J. S. (2020). Structural and simulation analysis of hotspot residues interactions of SARS-CoV 2 with human ACE2 receptor. *Journal of Biomolecular Structure and Dynamics*, 1–11. <https://doi.org/10.1080/07391102.2020.1773318>
- Vellingiri, B., Jayaramayya, K., Iyer, M., Narayanasamy, A., Govindasamy, V., Giridharan, B., Ganesan, S., Venugopal, A., Venkatesan, D., Ganesan, H., Rajagopalan, K., Rahman, P. K. S. M., Cho, S. G., Kumar, N. S., & Subramaniam, M. D. (2020). COVID-19: A promising cure for the global panic. *The Science of the Total Environment*, 725, 138277. <https://doi.org/10.1016/j.scitotenv.2020.138277>
- Verma, H. N., & Baranwal, V. K. (1983). Antiviral activity and the physical properties of the leaf extract of *Chenopodium ambrosoides* L. *Proceedings: Plant Sciences*, 92(6), 461–465. <https://doi.org/10.1007/BF03053019>
- Verma, H. N., Chowdhury, B., & Rastogi, P. (1984). Antiviral activity in leaf extracts of different Clerodendrum species. *Journal of Plant Diseases and Protection*, 91 (1), 34–41. <https://doi.org/10.2307/43382724>
- Yan, R., Zhang, Y., Li, Y., Xia, L., Guo, Y., & Zhou, Q. (2020). Structural basis for the recognition of SARS-CoV-2 by full-length human ACE2. *Science (New York, N.Y.)*, 367(6485), 1444–1448. <https://doi.org/10.1126/science.abb2762>
- Yao, X., Li, G., Bai, Q., Xu, H., & Lü, C. (2013). Taraxerol inhibits LPS-induced inflammatory responses through suppression of TAK1 and Akt activation. *International Immunopharmacology*, 15(2), 316–324. <https://doi.org/10.1016/j.intimp.2012.12.032>
- Yi, C., Sun, X., Ye, J., Ding, L., Liu, M., Yang, Z., Lu, X., Zhang, Y., Ma, L., Gu, W., Qu, A., Xu, J., Shi, Z., Ling, Z., & Sun, B. (2020). Key residues of the receptor binding motif in the spike protein of SARS-CoV-2 that interact with ACE2 and neutralizing antibodies. *Cellular and Molecular Immunology*, 17(6), 621–630. <https://doi.org/10.1038/s41423-020-0458-z>
- Yuan, M., Wu, N. C., Zhu, X., Lee, C. C. D., So, R. T. Y., Lv, H., Mok, C. K. P., & Wilson, I. A. (2020). A highly conserved cryptic epitope in the receptor binding domains of SARS-CoV-2 and SARS-CoV. *Science (New York, N.Y.)*, 368(6491), 630–633. <https://doi.org/10.1126/science.abb7269>